Applied Catalysis B: Environmental 258 (2019) 117933

Contents lists available at ScienceDirect

Applied Catalysis B: Environmental

journal homepage: www.elsevier.com/locate/apcatb

Conjugated porous polymer based on BOPHY dyes as photocatalyst under visible light

Carmen G. López-Calixto[a], Silvia Cabrera[b,c], Raúl Pérez-Ruiz[a,1], Mariam Barawi[a], José Alemán[b,d], Víctor A. de la Peña O'Shea[a,*], Marta Liras[a,*]

[a] Photoactivated Processes Unit, IMDEA Energy Institute, Ramón de la Sagra 3, 28935, Móstoles, Spain
[b] Institute for Advanced Research in Chemical Sciences (IAdChem), Universidad Autónoma de Madrid, 28049, Madrid, Spain
[c] Inorganic Chemistry Department, Módulo 7, Universidad Autónoma de Madrid, 28049, Madrid, Spain
[d] Organic Chemistry Department, Módulo 1 Universidad Autónoma de Madrid, 28049, Madrid, Spain

ARTICLE INFO

Keywords:
BOPHY
Conjugated porous polymer
Photoredox
Photocatalyst

ABSTRACT

The design and synthesis of new conjugated porous polymers based on BOPHY moiety (IEP-7 and IEP-8) which shows heterogeneous photocatalytic activity under visible light is reported. Both porous polymers are efficient photocatalysts in the selective oxidation of several sulfides into sulfoxides. The proposed mechanism is elucidated by steady state photolysis, fluorescence quenching and transient absorption spectroscopy, which follows a type I photosensitizing oxidation involving superoxide radical anion formation ($O_2^{-\cdot}$). Electron transfer from the sulfide derivative to the photocatalyst singlet exited state takes place, giving rise the corresponding radical ion pairs. Back electron transfer from oxygen molecular to the reduced BOPHY moiety with recovery of the photocatalyst, led to the formation of superoxide radical anion in an exergonic process.

1. Introduction

Photocatalytic chemical transformations using visible light as energy source have become a suitable 'greener' alternative in organic synthesis from an environmental point of view. Many of the common visible light homogeneous photocatalysts are based on Ru or Ir complexes and some metal-free organic dyes, enhancing their activities in the last years [1–7]. On the other hand, development of heterogeneous photocatalysts capable of absorbing in the visible range is nowadays a very important area of research that offers the opportunity of combining milder reaction conditions with facile separation, negligible contamination of products and photocatalyst recycling [8–13]. Thus, inorganic materials such as metal oxide semiconductors and supported plasmonic nanoparticles have been well-established [14–16] and, indeed, graphitic carbon nitride polymer g-C_3N_4 has been employed as organic photocatalytic material [17–19]. Analogously to g-C_3N_4, conjugated porous polymers, robust polymeric and cross-linked molecular structures present the advantage of a great structural diversity [20]; however, few examples of this type of materials as heterogeneous photocatalysts can be found in literature. For instance, polymers bearing appropriate chromophores such as azulene [21,22], carbazole [23], benzochalcogenadiazole [24], Rose Bengal [25], porphyrin [26] or BODIPY [27,28] have shown photocatalytic activity in organic transformations. Therefore, it will be of great interest to design and synthesize new polymers with alternative photoactive moieties able to be activated by visible light, in order to gain cost effectiveness of heterogeneous photocatalytic organic transformations.

Pioneering works by Ziegler and Jiao showed a practical and modular two-step synthesis of bis(difluoroboron)-1,2-bis((1H-pyrrol-2-yl)-methylene)hydrazines (BOPHYs) [29,30], a new highly fluorescent dyes containing two pyrrole-BF_2 groups on the structure. Since then, BOPHYs have experienced a rapid evolution in terms of applicability in diverse scientific fields such as solar cells [31,32], electrochemistry [33] or analytical chemistry [34]. Very recently, our research group has reported a proof-of-concept methodology for C—C coupling reactions catalyzed by a synchronized biphotonic process where a diiodo BOPHY-like derivative (compound **1b** in this work) has been used as photosensitizer [35]. Although BOPHYs are structurally similar to BODIPYs (Scheme 1), applications of conjugated porous polymers (CPPs) containing BOPHY as monomer in heterogeneous photocatalysis have not been reported yet. In the present work, new CPPs based on BOPHY moiety, **IEP-7** and **IEP-8**,(IEP as acronym of **IMDEA Energy Polymer**) have been successfully synthesized and fully characterized. Taking into account the optical properties of BOPHY dyes (**1a-c**), **IEP-7** and **IEP-8**

* Corresponding authors.
E-mail addresses: victor.delapenya@imdea.org (V.A. de la Peña O'Shea), marta.liras@imdea.org (M. Liras).
[1] Current address: Departamento de Química, Universitat Politècnica de València, Camino de Vera s/n, 46022, Valencia, Spain.

https://doi.org/10.1016/j.apcatb.2019.117933
Received 22 April 2019; Received in revised form 19 June 2019; Accepted 6 July 2019
Available online 08 July 2019

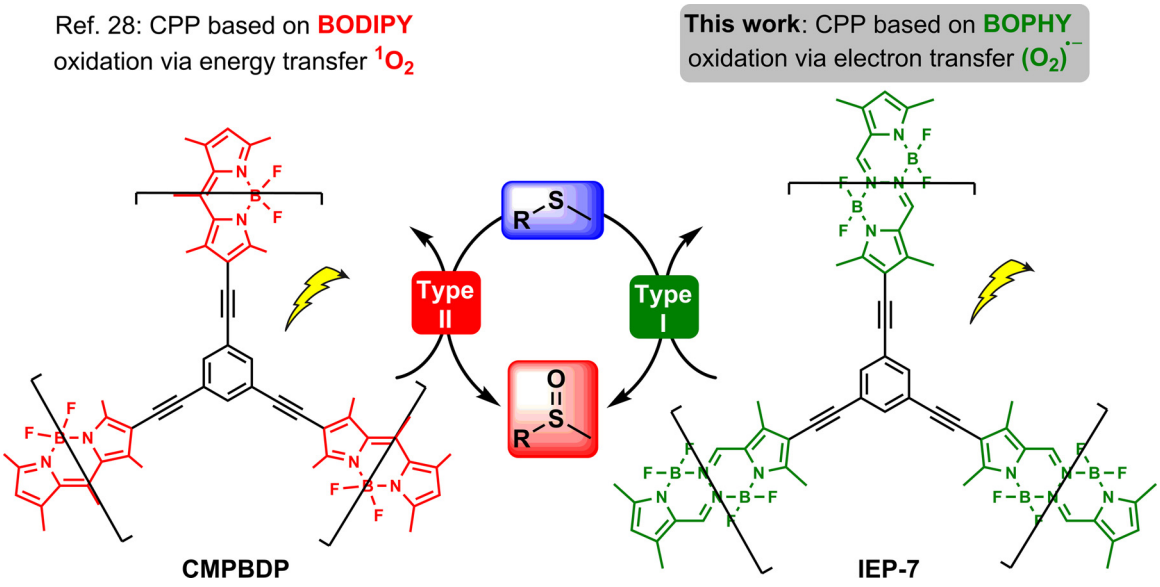

Scheme 1. Different strategies for the sulfide photooxidation by CPPs (CMPBDP = conjugated microporous polymer based on BODIPY dye).

have been proven, for the first time, as heterogeneous photocatalysts using visible light as energy source in the oxidation of several aromatic sulfide derivatives. Results have revealed selective formation of the corresponding sulfoxides. In parallel, **1a-c** have been also employed as homogeneous photocatalysts at the same oxidative reaction. Elucidation of mechanistic aspects related to the oxidation of sulfide derivatives by photoinduced electron transfer (PET) process has been analyzed by fluorescence quenching measurements. Besides laser flash photolysis (LFP) studies have provided clear evidences for the involvement of sulfide derivatives radical cation intermediates, point corroborated by DFT calculations. Therefore, Type I photooxidation occurring from the singlet excited state of BOPHY moiety appears to be the main operative pathway, in contrast to CPPs based on BODIPY dyes [28], which have been found to photocatalyze selective oxidation of thianisole *via* singlet oxygen (Scheme 1).

2. Experimental

Synthesis of IEP-7: BOPHY **1b** (591 mg, 1.00 mmol), 1,3,5-triethynylbenzene (100 mg, 0.67 mmol), $Pd(PPh_3)_4$ (31 mg, 0.03 mmol) and CuI (10 mg, 0.05 mmol) were placed in a Schlenk tube in DMF/Et_3N 1:1 (20 mL). The mixture was stirred under argon atmosphere at 80 °C during 4 days. The polymer obtained was filtered and washed with DCM, EtOAc, THF and ether. Then it was added to a solution of THF/H_2O (1:1) v/v with NaCN. The solution was stirred overnight. Finally, the polymer was filtered again and washed with H_2O and ACN. The compound **IEP-7** (386 mg, 82%) was obtained as a brown solid, insoluble in any solvent. Solid ^{13}C NMR (400 MHz) δ 124, 106, 92, 82, 11 ppm. Elemental analysis calculated to $C_{33}H_{24}B_3F_6N_6$: %C = 60.88; %H = 3.72; %N = 12.91; estimated: %C = 65.69; %H = 4.96; %N = 14.53

Synthesis IEP-8: BOPHY **1b** (469 mg, 0.79 mmol), monomer **3** (200 mg, 0.53 mmol), $Pd(PPh_3)_4$ (24 mg, 0.02 mmol) and CuI (8 mg, 0.04 mmol) were placed in a Schlenk tube in DMF/Et_3N 1:1 v/v (20 mL). The mixture was stirred under argon atmosphere at 80 °C during 10 days. The polymer obtained was filtered and washed with DCM, EtOAc, THF and ether. Then it was added to a solution of THF/H_2O (1:1) v/v with NaCN. The solution was stirred overnight. Finally, the polymer was filtered again and washed with H_2O and ACN. The compound **IEP-8** (460 mg, 99%) was obtained as a brown solid, insoluble in any solvent. Solid ^{13}C NMR (400 MHz) δ 138, 124, 103, 90, 81, 8 ppm. Elemental analysis calculated to $C_{54}H_{36}B_3F_6N_6$: %C = 69.66; %H = 4.13; %N = 9.56; estimated: %C = 73.14; %H = 5.19; %N = 7.95. Note that elemental analysis does not match with theoretical value because is very well-known that porous polymeric network and fluorine atoms present in BOPHY moiety lead to bad combustion and incorrect values of carbon.

3. Result and discussion

3.1. Synthesis

BOPHY dyes **1a-c** were prepared following a previously reported procedure where spectral data (see Supporting Information) were consistent according to literature [29,36]. Next, cross-coupling reaction of monomer **1b** with 1,3,5-triethynylbenzene (**2**) or 1,3,5-Tris(4-ethynylphenyl)benzene (**3**) through Sonogashira reaction [37] allowed the formation of **IEP-7** and **IEP8**, respectively (Scheme 2). The 3-days thermal reaction between **1b** and **2** or **3** (halogen atoms/triplet bonds 1:1 M ratio) in the presence of $Pd(PPh_3)_4$/CuI as catalyst/cocatalyst in Et_3N/DMF (1/1 v/v) under anaerobic conditions afforded the corresponding conjugated porous polymers in good yield (*ca.* 82% and 99%, respectively). Modification of halogen atoms/triplet bonds molar ratio led to loss of surface area (data not included), whereas prolongation of the thermal reaction time enhanced the total yield but not the porosity of the obtained material (data not included).

3.2. Characterization of CPPs based on BOPHY

The molecular structures of **IEP-7** and **IEP-8** were characterized by FTIR and ^{13}C-NMR in solid state. Thus, both FTIR spectra showed the C≡C stretching band located at 2194 cm^{-1}, indicating not only the condensation between the reactant units, but also the absence of the bands from the starting materials (Figs. 1 and S4 Supporting information). The work up included a treatment with aqueous sodium cyanide in order to remove totally residual Pd nanoparticles from the $Pd(PPh_3)_4$ catalyst (0.4 mol%) avoiding its interference in future experiments. In fact, ICP analysis revealed a negligible content of Pd in both **IEP-7** and **IEP-8** (0.02% wt and 0.007% wt, respectively). From solid state ^{13}C-NMR spectrum, a narrow peak at 11 ppm corresponding to the aliphatic C from BOPHY structure and two peaks at 82 and 92 ppm as result of the triple bond group were observed for **IEP-7**. The signals of the rest of aromatic carbons were localized at the interval 105–155 ppm where a narrow and intense band probably due to the CH from both BOPHY and

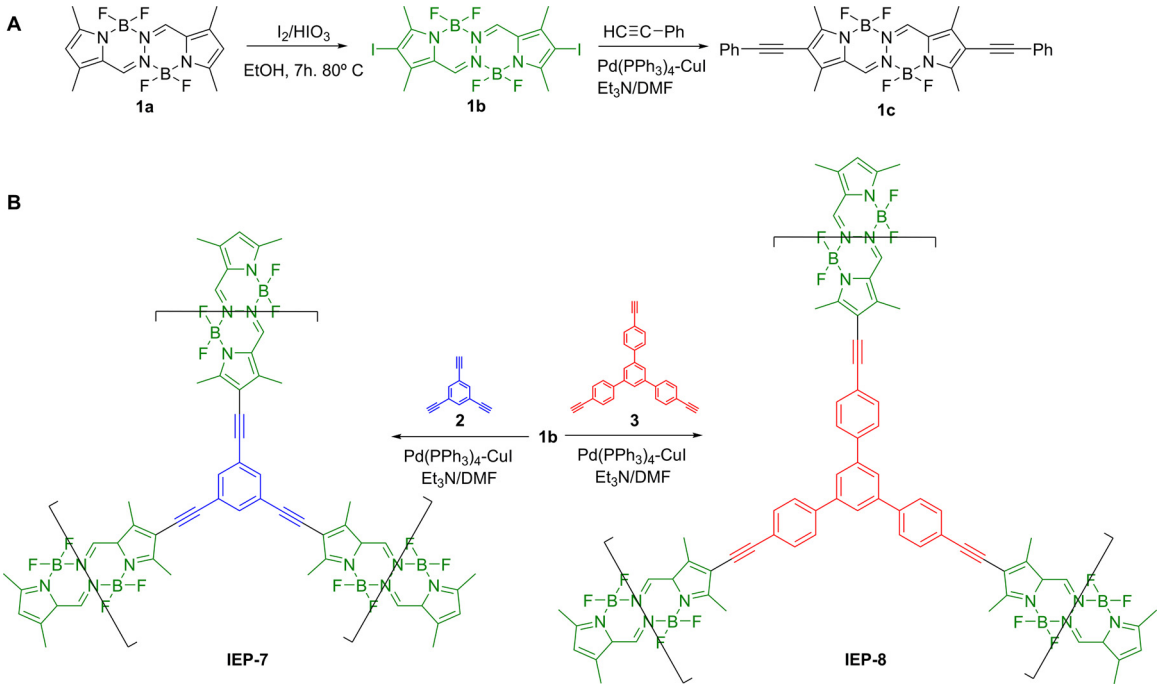

Scheme 2. Synthesis of **1a-ac** BOPHY dyes (A) and synthesis of Conjugated porous polymers (CPPs) based on BOPHY moiety, **IEP7** and **IEP-8** (B).

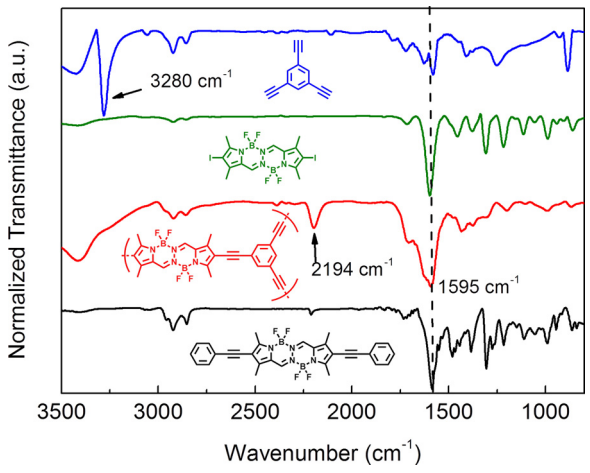

Fig. 1. FTIR spectra of **IEP-7** (red line), **1b** (green line), **2** (blue line) and model BOPHY dye **1c** (black line). (For interpretation of the references to colour in this figure legend, the reader is referred to the web version of this article.)

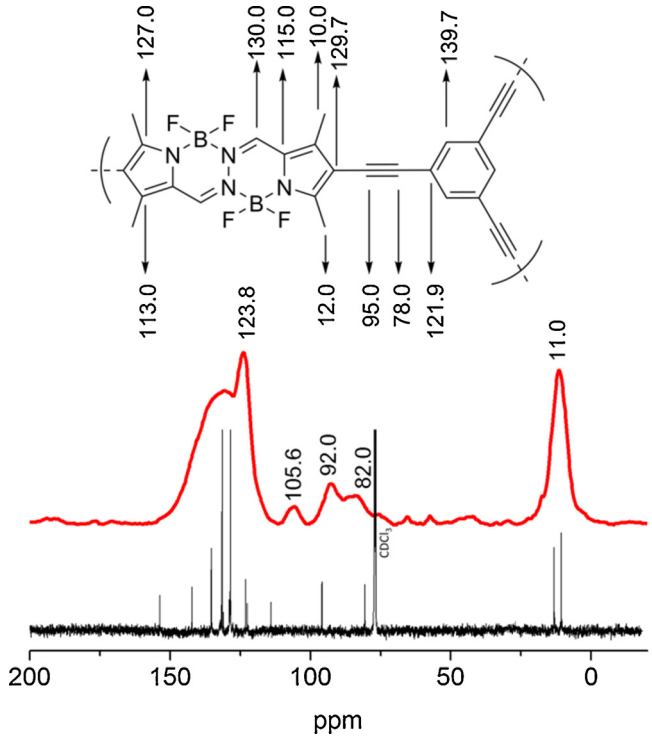

Fig. 2. Solid ^{13}C-NMR spectrum of **IEP-7** (red line). ^{13}C-NMR ($CDCl_3$) of **1c** spectrum (black) and theoretical assignment of **IEP-7** are included for comparative proposes. (For interpretation of the references to colour in this figure legend, the reader is referred to the web version of this article.)

benzene units was clearly detected (Fig. 2). Similar remarks were observed in the **IEP-8** case (Fig. S5, Supporting information)

The textural properties were analyzed by different techniques. The nitrogen sorption isotherms of both **IEP-7** and **IEP-8** materials fitted well to multilayer model from Brunauer-Emmett-Teller (BET) theory (Figs. S6–S7, Supporting information). Both **IEP-7** and **IEP-8** show less surface area (*ca.* 56 $m^2 g^{-1}$ and 69 $m^2 g^{-1}$, respectively) and porosity than their corresponding analogues polymers based on BODIPY synthesized in the same reaction conditions [22,23], presumably because BOPHY molecular structure was more orthogonal and longer than BODIPY dye. This would allow the interpenetration between the polymer branches, avoiding the laminar formation among polymer fragments. The mesoporous distribution of **IEP-7** was analyzed by Barrett-Joyner-Halenda (BJH) method affording 0.075 $cm^3 g^{-1}$ porous volume. The porous texture by SEM images shows canals and holes in **IEP-7** and flakes in **IEP-8** (Fig. 3). As expected, both polymers were amorphous polymers, based on data drawn from the powder X-ray diffraction (XRD) patterns (Fig. S8, Supporting information). The thermal stability of **IEP-7** by thermogravimetry under anaerobic and aerobic conditions was analyzed (Fig. S9, Supporting information). Under inert atmosphere, the thermogram of **IEP-7** depicts a high thermostability with no degradation. However, the thermodegradation of **IEP-7** under air conditions produced decomposition in two steps (*ca.* onset 300 °C and 468 °C), presumably the first one corresponding to the

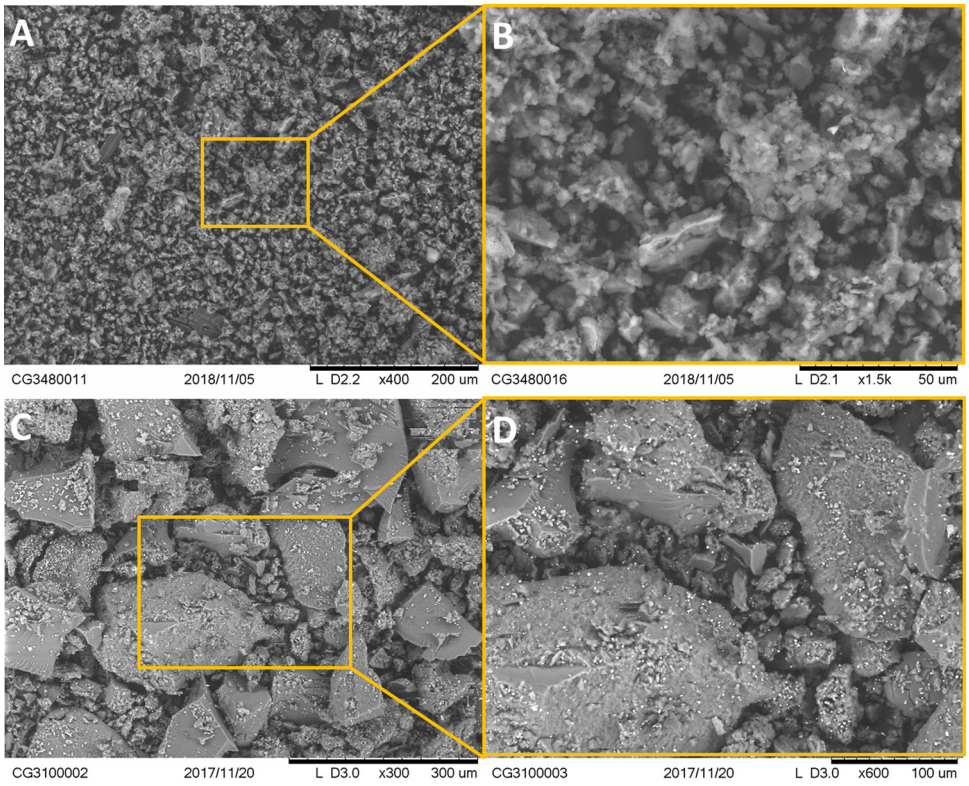

Fig. 3. SEM images of **IEP-7** (A) and **IEP-8** (C) and its magnification (B and D, respectively).

most labile BOPHY moiety, with only 6–8% of solid residue. **IEP-8** shows similar thermostability (Fig. S10, Supporting information).

Regarding optical characterization, the photophysical properties of **1a-c**, which include absorption/emission bands, molar absorption coefficients, fluorescence quantum yields, singlet lifetimes and energy, were studied in different solvents (see Table S1 and Fig. S11, Supporting information). The obtained results were similar to those previously reported [36]. Note that substituted BOPHYs **1b** and **1c** exhibited red-shifted emissions together with a significant drop in the fluorescence quantum yields in comparison with **1a**. On the other hand, both **IEPs** possessed the $\pi-\pi^*$ transition of triethynylbenzene (300 nm) and an absorption band at *ca.* 380 nm assigned to the $S_0 \rightarrow S_1$ transition of the BOPHY chromophore in dispersed acetonitrile solution (Fig. 4). A hypsochromic shift of this transition was actually appreciated with respect to the BOPHY chromophore **1a**, and a similar trend was observed in the emission spectra.

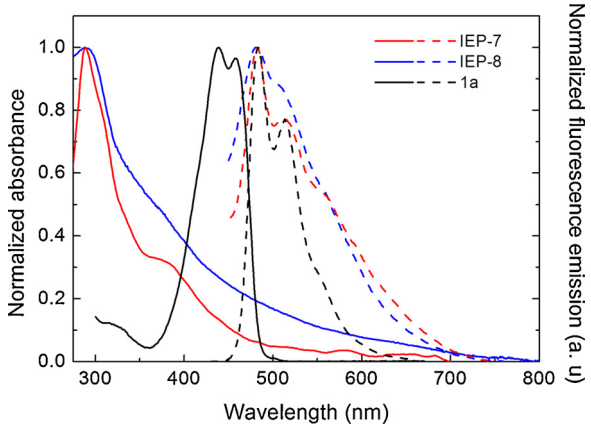

Fig. 4. Normalized absorption (solid lines) and fluorescence emission (dash lines) of **IEP-7** (red), **IEP-8** (blue) and BOPHY compound **1a** (black) in acetonitrile. Excitation wavelength 420 nm. (For interpretation of the references to colour in this figure legend, the reader is referred to the web version of this article.)

Electrochemical characterization of **1a-c** BOPHY dyes and both polymers was performed by means of cyclic voltammetry measurement (Figs. 5A and S13). Only the oxidation of **1a** and **1b** and the reduction of **IEP-7** and **IEP-8** are reversible; whereas the reduction of **1a**, **1b** and **1c** as well as the oxidation of **1c**, **IEP-7** and **IEP-8** are irreversible. HOMO/LUMO energy levels positions of **1a-c** dyes and valence/conduction bands edges of both polymeric networks were calculated based on these data (Fig. 5B, and Supporting information). Notice that, as expected, the electronic band gap is bigger than the optical one (see Table S2 and Fig. S12 in Supporting information) due probably to the exciton binding energy, which can be calculated [38].

3.3. Photocatalytic activity

To investigate whether conjugated porous polymer based on BOPHY moiety and dyes **1a-c** could act as heterogeneous and homogeneous photocatalysts respectively, we selected as model photoreaction the oxidation of sulfides to the corresponding sulfoxides, which are very important compounds in organic synthesis, medicinal chemistry and natural products [36,15,16]. *A priori*, BOPHY derivatives may behave as photooxidizing agents based on recent reports on analogous BODIPYs [28]. We first studied the oxidation of methyl *p*-tolylsulfide (**4a**) in the presence of catalytic amounts of **IEP-7** under green light irradiation (see Figs. S1–S2 in Supporting information) in aerated EtOH/water solvent ('greener' conditions), leading to good conversion of the starting material (Table 1, entries 1–4). Note that this reaction is thermodynamically possible taking into account the E_0^{ox} (**4a**/**4a**$^{+\cdot}$) regarding **IEP-7** energy edge band positions (Fig. 5B). The optimal conditions for achieving the photooxidation of sulfide **4a** at 24 h of reaction implied loading of 1 mol% of **IEP-7** (Table 1, entry 2). It is worth mentioning that a control experiment using **IEP-7** before Pd cleaning treatment showed the same result (Table 1, entry 12), confirming that the

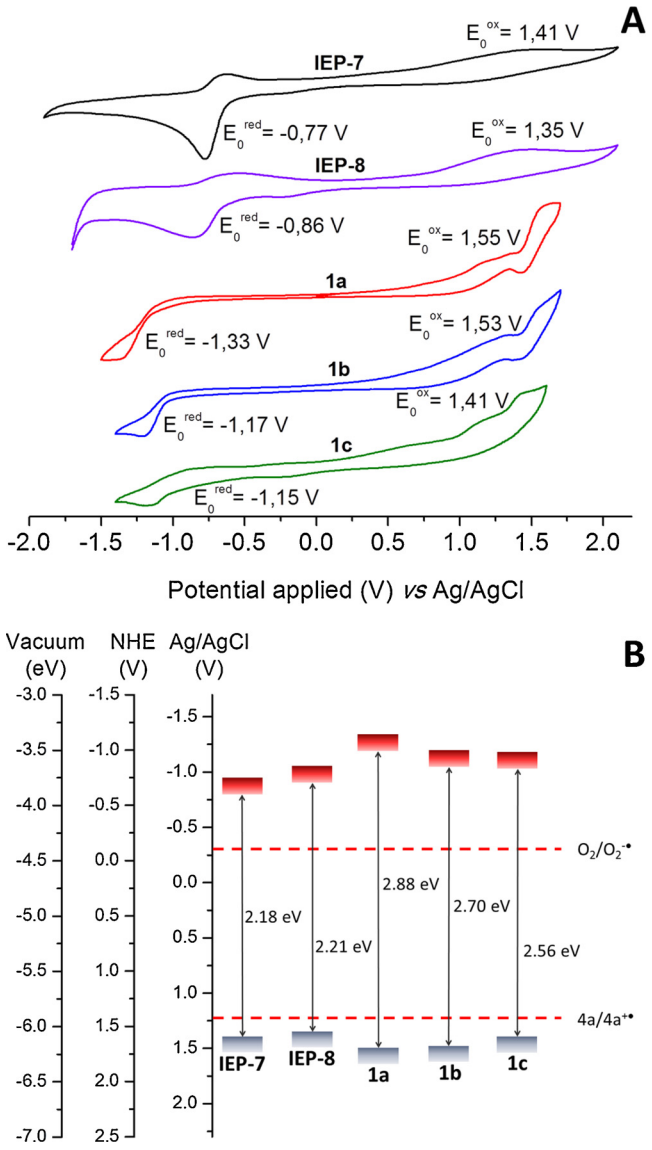

Fig. 5. (A) Cyclic voltammetry of **IEP-7** and **IEP-8** deposited on platinum disc electrode as well as 1 mM solution of **1a-c** measured in acetonitrile containing 0.1 M $TBAPF_6$ as electrolyte. The scan rate was 50 mVs^{-1} in all cases. (B) HOMO/LUMO energy levels of **1a-c** and valence/conduction bands of **IEP-7** and **IEP-8** in front of the $O_2/O_2^{\cdot-}$ and **4a**/**4a**$^{+\cdot}$ redox pairs.

presence of metal nanoparticles did not boost the corresponding oxidation reaction. Besides, **IEP-8** afforded lower conversion from **4a** sulfide (*ca.* 55%) in comparison with **IEP-7** (Table 1, entry 4 *vs* entry 5), mainly due to the lesser oxidant capabilities of **IEP-8** (Fig. 5B) where the HOMO position is localized at higher energies than that of **IEP-7**.

More importantly, the reusability of **IEP-7** polymer retained 47 ± 8% of sulfide conversion after 4 cycles tested. Thus, a diminished activity of **IEP-7** was observed on the second run while maintaining it during the next third and fourth run (Fig. S3, Supporting information). It could be explained in terms of adsorption where some amount of the starting material would be adsorbed onto the heterogeneous catalyst in the first run, affecting somehow for the second cycle. In fact, FTIR spectrum before and after recycling experiment exhibit the same bands, indicating the stability of the material under reaction conditions.

We were also interested in exploring the behavior of dyes **1a-c** as photocatalyts in homogeneous phase, which has not been reported to date. After 24 h of reaction, all of them showed 100% conversion from **4a** to **5a** (data not showed in the Table 1). In order to study reactivity

Table 1
Photocatalyst screening and optimization of reaction conditions.[a]

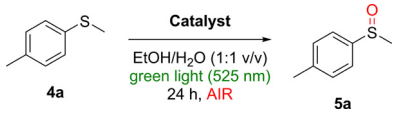

Entry	Catalyst	% mol	Time (h)	Conv. (%)[b]
1	**IEP-7**	0.7	24	48
2	**IEP-7**	1.0	24	69
3	**IEP-7**	1.2	24	67
4	**IEP-7**	2.5	24	77
5	**IEP-8**	1.0	24	55
6	**1a**	1.2	8	59
7	**1a**	0.7	8	75
8	**1b**	0.7	8	67
9	**1c**	0.7	8	43
10	**IEP-7**	1.0	24	68[c]
11	**IEP-7**	1.0	24	11[d]
12	**IEP-7-Pd**[e]	1.0	24	67

[a] All reactions were carried out using **4a** (0.3 mmol) in 2 ml of a mixture EtOH/H_2O (1:1 v/v) under green-LED irradiation (λ_{em} = 525 nm).
[b] Conversion yield determined by ^{1}H NMR. analysis of the crude mixture.
[c] With DABCO (0.15 mmol).
[d] With benzoquinone (0.15 mmol).
[e] Control experiment using **IEP-7** before Pd cleaning treatment.

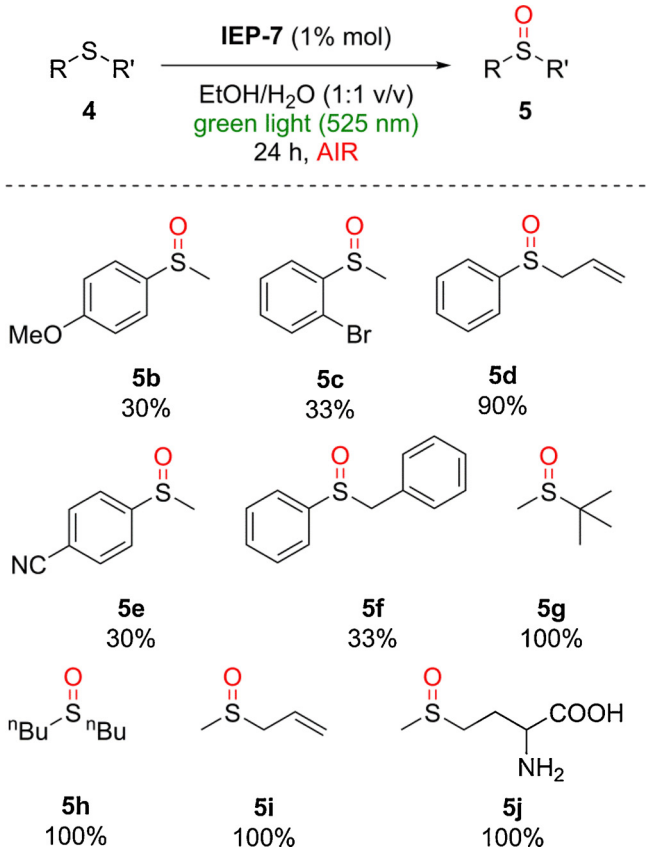

Scheme 3. Some examples supporting the photocatalytic activity of **IEP-7**.

differences between them, the irradiation time was decreased to 8 h. At 8 h of reaction time, good to excellence conversions of **4a** selectively to **5a** were detected in all cases (Table 1, entries 6–9). It is worth mentioning that 1 mol% of **IEP-7** heterogeneous catalyst is equivalent to 0.7 mol% of homogeneous one. However, the increase of the amount of catalyst **1a** to 1.2 mol% did not lead to an increment in **4a** conversion (Table 1, entry 6). Furthermore, the photocatalytic efficiency followed

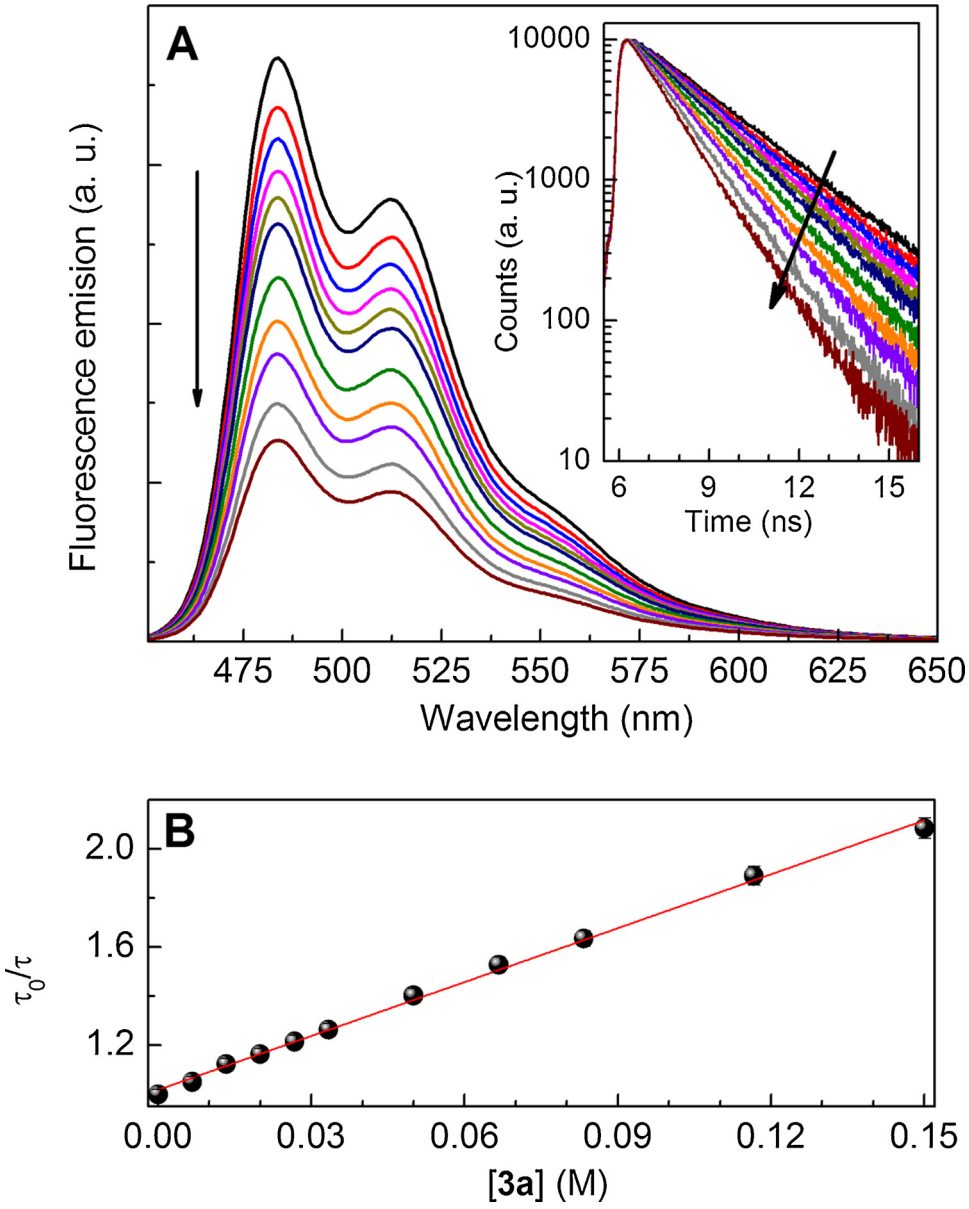

Fig. 6. A: Steady-state quenching of **1a** fluorescence in the presence of increasing amounts of **4a** (up to 0.15 M); inset: time-resolved quenching of **1a** fluorescence upon increasing concentrations of **4a** (up to 0.15 M). **B**: Stern-Volmer plot to obtain $k_q(S_1)$.

the order **1a** > **1b** > **1c** under the same conditions (Table 1, entries 7–9). This reactivity order seems to be contrary to expectations if the reaction occurs *via* generation of singlet oxygen by triplet energy transfer since fluorescence quantum yield of **1a** was close to the unit meanwhile the triplet state of **1c** is presumably most likely by heavy atom effect. In the absence of either component (light, photocatalyst, non-aerated conditions), no sulfoxidation was observed (control experiments no included in Table 1).

Once, **IEP-7** was established as suitable photooxidizing catalyst, the reaction scope was studied with several sulfide derivatives (Scheme 3). All the reactions were carried out using the optimal reaction conditions (Table 1, entry 2). Thus, sulfides containing electron-donating groups at the aryl moiety (**4b**) as well as electron withdrawing groups (**4c** and **4e**) were oxidized with moderate conversions (*ca.* 30%). Aryl-sulfides containing an allyl group (**4d**) or a benzyl group (**4f**), instead of the methyl group, were chemoselectively oxidized to the corresponding sulfoxides, without detection of benzaldehyde, sulfone or unidentified byproducts as it was found with some homogeneous catalytic systems [39]. Besides, dialkyl sulfides (**4g**-**4i**) or even the unprotected methionine aminoacids (**4j**) were fully converted into their corresponding sulfoxides (**5g-5j**). Importantly, all the studied oxidations were completely chemoselective and neither sulfone nor any other byproducts were detected by ^{1}H-NMR in the reaction mixture.

3.4. Mechanism investigations

3.4.1. Steady-state photolysis

To elucidate at first stage mechanistic hints of the sulfoxidation reaction, involving a photoinduced electron transfer (PET) process, steady-state photolysis experiments were performed in the presence of DABCO (an efficient singlet oxygen quencher) or benzoquinone (BQ), which is a trapping agent for $O_2^{\cdot -}$. Interestingly, the heterogeneous photocatalytic oxidation of **4a** was not affected by the presence of DABCO (Table 1, entry 10). By contrast, in the case of BQ the oxidation rate drastically decreased with almost negligible conversion to product (Table 1, entry 11). From these data, it appeared conclusive that $O_2^{\cdot -}$ played a key role as transient intermediate in the PET process. Furthermore, these findings were in good agreement with abovementioned

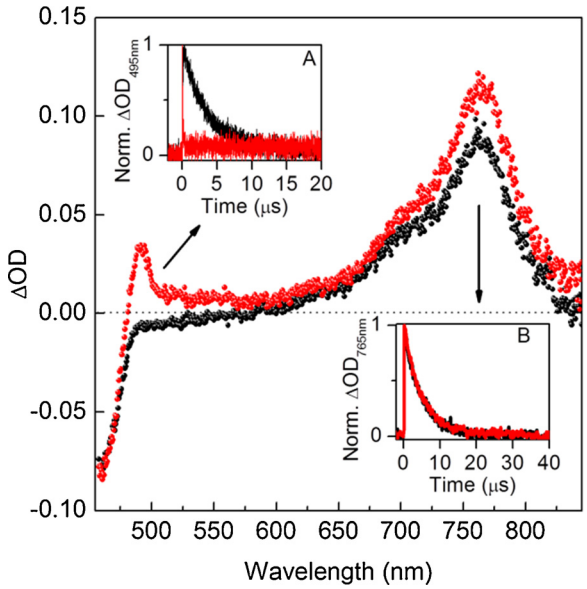

Fig. 7. Laser flash photolysis (λ_{exc} = 420 nm) of **1a** (0.05 mM) in N_2/Acetonitrile monitored 20 ns after laser pulse in the absence (black) and in the presence of 0.15 M **4a** (red). Inset A: Decay monitored at 495 nm after laser flash photolysis (λ_{exc} = 420 nm/ACN) for **1a** (0.05 mM) + **4a** (0.15 M) under nitrogen (black) and air (red) conditions. Inset B: Decays monitored at 765 nm after laser flash photolysis (λ_{exc} = 420 nm, N_2/ACN) for **1a** (0.05 mM) in the absence (black) and in the presence of 0.15 M **4a** (red). (For interpretation of the references to colour in this figure legend, the reader is referred to the web version of this article.)

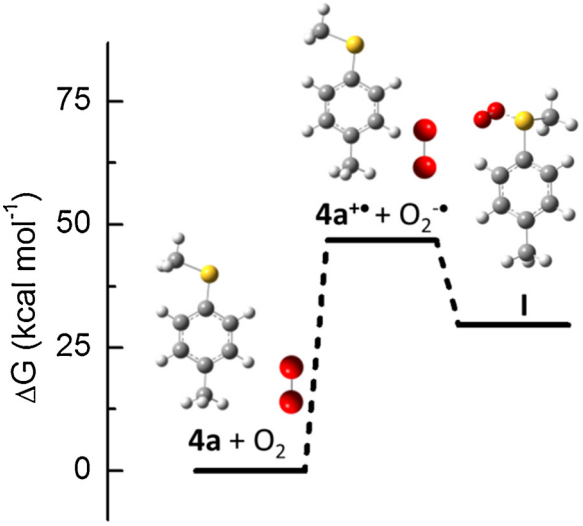

Fig. 8. Energy profile for the reaction of methyl *p*-tolylsulfide (**4a**) and oxygen in acetonitrile media.

observations where catalyst **1a** exhibited the best photocatalytic activity.

To gain further insight into the mechanistic aspects, an integrated investigation combining fluorescence quenching studies, laser flash photolysis experiments and theoretical calculations was carried out.

3.4.2. *Fluorescence quenching*

To disclose the nature of the excited state involved in the PET process, **1a** emission was recorded in the presence of increasing amounts of **4a**. The steady-state fluorescence intensity gradually decreased while preserving its characteristic shape (Fig. 6A), indicating the potential participation of the excited state in the PET process. To unequivocally demonstrate the participation of the **1a** singlet state (^{1}**1a***) in the photooxidation, time-resolved emission measurements were also achieved with different concentrations of **4a** (Fig. 6A, inset). Results clearly showed that electron transfer from ^{1}**1a*** corresponded to a dynamic process, ruling out any formation of charge transfer complexes in the ground state. The quenching rate constant, $k_q(S_1)$ was determined by means of the Stern-Volmer analysis (Fig. 6B) [40]. Taking into account the obtained Stern-Volmer constant (K_{SV} = 7.3 M^{-1}) and the singlet lifetime of **1a** (τ_S = 2.7 ns in air), $k_q(S_1)$ was found to be 2.7 × 10^9 $M^{-1}s^{-1}$, confirming that **4a** quenched ^{1}**1a*** at a nearly diffusion controlled rate. It is interesting to mention that changes in the ^{1}**1a*** fluorescence lifetime was negligible under either aerobic or anaerobic conditions (Figure S14, Supporting Information).

Furthermore, estimation of the free energy change associated with ET from ^{1}**1a*** to **4a** ($\Delta G_{ET}(S_1)$ = − 8.75 kcal mol^{-1}) using the Rehm-Weller equation [41] was compatible with generation of **4a**$^{\cdot+}$ (see Supporting Information for details). Therefore, all these kinetic and thermodynamic data coupled energy levels depicts in Fig. 5B proven in an unambiguously way that the initial step of the reaction involved the generation of the radical ion pair **1a**$^{\cdot-}$/**4a**$^{\cdot+}$.

3.4.3. *Transient absorption spectroscopy (TAS)*

Experimental evidence of the generation of radical cation **4a**$^{\cdot+}$ in the initial step of the reaction was demonstrated by TAS. Irradiation of **1a** at 420 nm (N_2/Acetonitrile) resulted in a peak centered at 765 nm (Fig. 7) assigned to the characteristic triplet-triplet absorption of **1a** [36]. This experiment was also carried out in the presence of **4a** in order to identify possible transient reaction intermediates. A new band at 500 nm was clearly observed together with a slightly enhancement of the centered 765 nm band. These were safely ascribed to the formation of dimer radical cation from the corresponding aromatic sulfide,

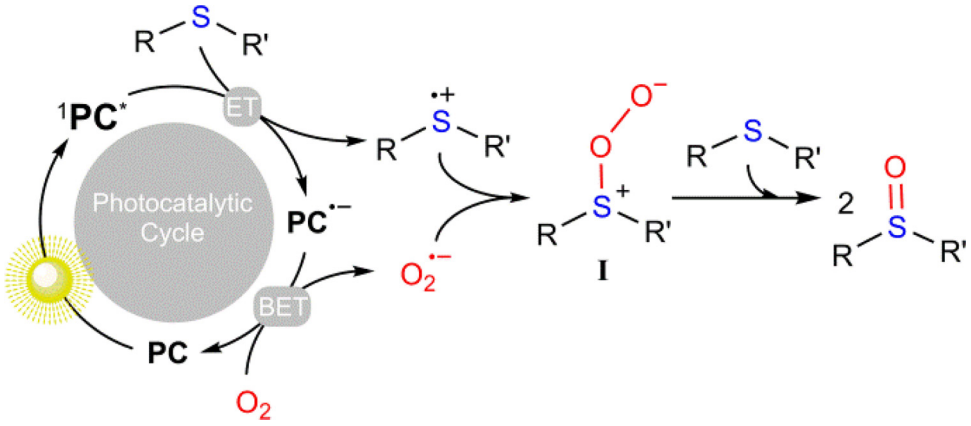

Scheme 4. Plausible mechanism for the photocatalytic oxidation of sulfide derivatives (ET = electron transfer; BET = back electron transfer).

$(\mathbf{4a})_2^{\cdot+}$, on the basis of literature data [39,42].

Under high concentration conditions, sulfide radical cations are capable to form dimers by association with ground-state molecules. Therefore, these findings confirmed the PET nature of the process. To check whether **1a** triplet (^{3}**1a***) may be involved in the PET process, existence of observable triplet quenching of **1a** by **4a** was required as foremost condition. Such triplet quenching did not actually occur (Fig. 6B) and consequently oxidation of **4a** by ^{3}**1a*** did not take place. Finally, TAS investigations also provided key information related to the reaction mechanism, where the whole quenching of the transient species at 495 nm in aerobic conditions (Inset A Fig. 7) together with steady-state irradiations in the presence of DABCO and benzoquinone (Table 1, entries 10–11), clearly supported the reaction of sulfide radical cation and O_2. In addition, electron paramagnetic resonance (EPR) analysis further confirmed the involvement of O_2 as key intermediate (Fig. S7, Supporting information).

3.4.4. Proposed reaction mechanism

In agreement with the above data, a plausible mechanism is depicted in Scheme 4. The process commences with the selective irradiation to the photocatalyst that, after visible light absorption, forms its excited singlet state. Electron transfer from the sulfide derivative to the photocatalyst singlet takes place, giving rise the corresponding radical ion pairs. Back electron transfer (BET) from oxygen molecular to the reduced BOPHY moiety with recovery of the photocatalyst, gave rise to the formation of superoxide radical anion (ΔG of this process appears to be exergonic based on redox potentials, see Supporting Information for more details) which could react with sulfide radical cation to form final products *via* intermediate **I**. To support this proposed reaction mechanism, theoretical calculations based on DFT methods at the B3LYP/6-31 + G(2d,p) level of theory (see details in Supporting information) were performed to determine the energy profile from the radical cation of methyl *p*-tolylsulfide ($\mathbf{4a}^{\cdot+}$) as model in acetonitrile solvent (Fig. 8). These calculations confirmed the intermediate I formation, showing a O—O bond length value of 1.484 Å and 1.622 Å for S—O bond length; these results are in agreement with previously reported data [43,44].

4. Conclusions

New conjugated porous polymers based on BOPHY dye moiety, **IEP-7** and **IEP-8** have been synthesized. The photocatalytic under visible light irradiation (*ca.* 525 nm) behaviors of both polymers and models BOPHY dyes **1a-1c** have been checked in the oxidation of several sulfides into sulfoxides. A wide scope using **IEP-7** as heterogeneous photocatalyst has been corroborated as well as the retention of the photocatalytic activity after four cycles. The Type I oxidative mechanism *via* O_2, general for BOPHY dyes, has been corroborate by steady state, quenching and laser flash photolysis experiments. Noteworthy, this behavior is opposite to the former observed Type II mechanism *via* $O_2{}^1$ for conjugated analogues porous polymer based on BODIPY.

Acknowledgements

This work received financial support from the Ministerio de Economía y Competitividad (MINECO) from Spain through the Projects ENE2016-79608-C2-1-R and CTQ2015-64561-R, RTI2018-095038-B-I00 (AEI/FEDER, UE) and the regional government of “Comunidad de Madrid” and European Structural Funds for their financial support to FotoArt-CM project (S2018/NMT-4367). Also, M. L and M. B thank to MINECO and European Social Fund for a Ramón y Cajal contract (RyC-2015-18677) and Juan de la Cierva Formación contract (FJCI-2016-30567), respectively. R.P.-R. thanks the regional government of “Comunidad de Madrid” (Talent Attraction Program, 2016-T1/AMB-1275) and Valencian Community (CIDEGENT/2018/044).

Appendix A. Supplementary data

Supplementary material related to this article can be found, in the online version, at doi:https://doi.org/10.1016/j.apcatb.2019.117933.

References

[1] J.-R. Chen, X.-Q. Hu, L.-Q. Lu, W.-J. Xiao, Visible light photoredox-controlled reactions of N-radicals and radical ions, Chem. Soc. Rev. 45 (2016) 2044–2056, https://doi.org/10.1039/C5CS00655D.
[2] C. Boyer, Organic photocatalysts for cleaner polymer synthesis, Science 352 (2016) 1053–1054.
[3] N.A. Romero, D.A. Nicewicz, Organic photoredox catalysis, Chem. Rev. 116 (2016) 10075–10166, https://doi.org/10.1021/acs.chemrev.6b00057.
[4] B. König, Photocatalysis in organic synthesis – past, present, and future, Eur. J. Org. Chem. (2017) 1979–1981, https://doi.org/10.1002/ejoc.201700420.
[5] M.L. Marin, L. Santos-juanes, A. Arques, A.M. Amat, M.A. Miranda, Organic photocatalysts for the oxidation of pollutants and model compounds, Chem. Rev. 112 (2012) 1710–1750.
[6] D.A. Nicewicz, D.W.C. MacMillan, Merging photoredox catalysis with organocatalysis: the direct asymmetric alkylation of aldehydes, Science 322 (2008) 77–80, https://doi.org/10.1126/science.1161976.
[7] X. Lang, J. Zhao, X. Chen, Cooperative photoredox catalysis, Chem. Soc. Rev. 45 (2016) 3026–3038, https://doi.org/10.1039/c5cs00659g.
[8] J.C. Colmenares, R. Luque, Heterogeneous photocatalytic nanomaterials: transformations of biomass-derived compounds, Chem. Soc. Rev. 43 (2014) 765–778, https://doi.org/10.1039/c3cs60262a.
[9] Y. Qu, X. Duan, Progress, challenge and perspective of heterogeneous photocatalysts, Chem. Soc. Rev. 42 (2013) 2568–2580, https://doi.org/10.1039/C2CS35355E.
[10] H. Wang, L. Zhang, Z. Chen, J. Hu, S. Li, Semiconductor heterojunction photocatalysts: design, construction, and photocatalytic, Chem. Soc. Rev. 43 (2014) 5234–5244, https://doi.org/10.1039/c4cs00126e.
[11] S. Xie, Q. Zhang, G. Liu, Y. Wang, Photocatalytic and photoelectrocatalytic reduction of CO2 using heterogeneous catalysts with controlled nanostructures, Chem. Commun. 52 (2016) 35–59, https://doi.org/10.1039/C5CC07613G.
[12] X. Lang, X. Chen, J. Zhao, Heterogeneous visible light photocatalysis for selective organic transformations, Chem. Soc. Rev. 43 (2014) 473–486, https://doi.org/10.1039/C3CS60188A.
[13] F. Fresno, R. Portela, S. Suárez, J.M. Coronado, Photocatalytic materials: recent achievements and near future trends, J. Mater. Chem. A 2 (2014) 2863–2884, https://doi.org/10.1039/c3ta13793g.
[14] H. Hao, X. Lang, Metal sulfide photocatalysis: visible-light-induced organic transformations, ChemCatChem 11 (2019) 1378–1393, https://doi.org/10.1002/cctc.201801773.
[15] H. Hao, Z. Wang, J.L. Shi, X. Li, X. Lang, Improving the visible light photocatalytic aerobic oxidation of sulfides into sulfoxides on dye-sensitized TiO2, ChemCatChem 10 (2018) 4545–4554, https://doi.org/10.1002/cctc.201801304.
[16] X. Lang, J. Zhao, X. Chen, Visible-light-Induced photoredox catalysis of dye-sensitized titanium dioxide: selective aerobic oxidation of organic sulfides, Angew. Chem. - Int. Ed. 55 (2016) 4697–4700, https://doi.org/10.1002/anie.201600405.
[17] Y. Zheng, L. Lin, B. Wang, X. Wang, Graphitic carbon nitride polymers toward sustainable photoredox catalysis, Angew. Chem. - Int. Ed. 54 (2015) 12868–12884, https://doi.org/10.1002/anie.201501788.
[18] A. Savateev, M. Antonietti, Heterogeneous organocatalysis for photoredox chemistry, ACS Catal. 8 (2018) 9790–9808, https://doi.org/10.1021/acscatal.8b02595.
[19] W.J. Ong, L.L. Tan, Y.H. Ng, S.T. Yong, S.P. Chai, Graphitic carbon nitride (g-C3N4)-based photocatalysts for artificial photosynthesis and environmental remediation: are we a step closer to achieving sustainability? Chem. Rev. 116 (2016) 7159–7329, https://doi.org/10.1021/acs.chemrev.6b00075.
[20] H. Bildirir, V.G. Gregoriou, A. Avgeropoulos, U. Scherf, C.L. Chochos, Materials horizons porous organic polymers as emerging new materials for organic photovoltaic applications: current status and future challenges, Mater. Horiz. 4 (2017) 546–556, https://doi.org/10.1039/C6MH00570E.
[21] S. Ghasimi, K. Landfester, K.A.I. Zhang, Water compatible conjugated microporous polyazulene networks as visible-light photocatalysts in aqueous medium, ChemCatChem 8 (2016) 694–698, https://doi.org/10.1002/cctc.201501102.
[22] S. Ghasimi, S.A. Bretschneider, W. Huang, K. Landfester, K.A.I. Zhang, A conjugated microporous polymer for palladium-free, visible light-promoted photocatalytic stille-type coupling reactions, Adv. Sci. 4 (2017) 1700101, , https://doi.org/10.1002/advs.201700101.
[23] C. Su, R. Tandiana, B. Tian, A. Sengupta, W. Tang, J. Su, K.P. Loh, Visible-light photocatalysis of aerobic oxidation reactions using carbazolic conjugated microporous polymers, ACS Catal. (2016) 3594–3599, https://doi.org/10.1021/acscatal.6b00443.
[24] R. Li, J. Byun, W. Huang, C. Ayed, L. Wang, K.A.I. Zhang, Poly(benzothiadiazoles) and their derivatives as heterogeneous photocatalysts for visible-light-driven chemical transformations, ACS Catal. 8 (2018) 4735–4750, https://doi.org/10.1021/acscatal.8b00407.
[25] J.-X. Jiang, Y. Li, X. Wu, J. Xiao, D.J. Adams, A.I. Cooper, Conjugated microporous polymers with rose bengal dye for highly efficient heterogeneous organo-photocatalysis, Macromolecules 46 (2013) 8779–8783, https://doi.org/10.1021/ma402104h.
[26] R. Chen, J.L. Shi, Y. Ma, G. Lin, X. Lang, C. Wang, Designed synthesis of a 2D

porphyrin-based sp 2 carbon-conjugated covalent organic framework for heterogeneous photocatalysis, Angew. Chem. - Int. Ed. 58 (2019) 6430–6434, https://doi.org/10.1002/anie.201902543.
[27] M. Liras, M. Pintado-Sierra, M. Iglesias, F. Sánchez, Deprotection strategy of a BODIPY conjugated porous polymer to obtain heterogeneous (dipyrrin)(bipyridine) ruthenium(II) visible light photocatalyst, J. Mater. Chem. A 4 (2016) 17274–17278, https://doi.org/10.1039/C6TA07696C.
[28] M. Liras, M. Iglesias, F. Sánchez, Conjugated microporous polymers incorporating BODIPY moieties as light-emitting materials and recyclable visible-light photocatalysts, Macromolecules 49 (2016) 1666–1673, https://doi.org/10.1021/acs.macromol.5b02511.
[29] I.-S. Tamgho, A. Hasheminasab, J.T. Engle, V.N. Nemykin, C.J. Ziegler, A new highly fluorescent and symmetric pyrrole–BF2 chromophore: BOPHY, J. Am. Chem. Soc. 136 (2014) 5623–5626, https://doi.org/10.1021/ja502477a.
[30] C. Yu, L. Jiao, P. Zhang, Z. Feng, C. Cheng, Y. Wei, X. Mu, E. Hao, Highly fluorescent BF 2 complexes of hydrazine − Schiff base linked bispyrrole, Org. Lett. (2014) 3048–3051.
[31] Q. Huaulmé, A. Mirloup, P. Retailleau, R. Ziessel, Synthesis of highly functionalized BOPHY chromophores displaying large stokes shifts, Org. Lett. 17 (2015) 2246–2249, https://doi.org/10.1021/acs.orglett.5b00858.
[32] A. Mirloup, Q. Huaulmé, N. Leclerc, P. Lévêque, T. Heiser, P. Retailleau, R. Ziessel, Thienyl-BOPHY dyes as promising templates for bulk heterojunction solar cells, Chem. Commun. 51 (2015) 14742–14745, https://doi.org/10.1039/C5CC05095B.
[33] H.M. Rhoda, K. Chanawanno, A.J. King, Y.V. Zatsikha, C.J. Ziegler, V.N. Nemykin, Unusually strong long-distance metal-metal coupling in bis(ferrocene)-containing BOPHY: an introduction to organometallic BOPHYs, Chem. - A Eur. J. 21 (2015) 18043–18046, https://doi.org/10.1002/chem.201504004.
[34] X.-D. Jiang, Y. Su, S. Yue, C. Li, H. Yu, H. Zhang, C.-L. Sun, L.-J. Xiao, Synthesis of mono-(p-dimethylamino)styryl-containing BOPHY dye for a turn-on pH sensor, RSC Adv. 5 (2015) 16735–16739, https://doi.org/10.1039/C4RA15914D.
[35] C.G. López-Calixto, M. Liras, V.A. De La Peña O'Shea, R. Pérez-Ruiz, Synchronized biphotonic process triggering C—C coupling catalytic reaction, Appl. Catal. B Environ. 237 (2018) 18–23, https://doi.org/10.1016/j.apcatb.2018.05.062.
[36] X. Li, G. Ji, Y.A. Son, Tunable emission of hydrazine-containing bipyrrole fluoroboron complexes by linear extension, Dyes Pigm. 124 (2016) 232–240, https://doi.org/10.1016/j.dyepig.2015.09.022.
[37] J.-X. Jiang, F. Su, A. Trewin, C.D. Wood, H. Niu, J.T. a Jones, Y.Z. Khimyak, A.I. Cooper, Synthetic control of the pore dimension and surface area in conjugated microporous polymer and copolymer networks, J. Am. Chem. Soc. 130 (2008) 7710–7720, https://doi.org/10.1021/ja8010176.
[38] A.J. Molina-Mendoza, M. Barawi, R. Biele, E. Flores, J.R. Ares, C. Sánchez, G. Rubio-Bollinger, N. Agraït, R. D'Agosta, I.J. Ferrer, A. Castellanos-Gomez, Electronic bandgap and exciton binding energy of layered semiconductor TiS3, Adv. Electron. Mater. 1 (2015) 1–6, https://doi.org/10.1002/aelm.201500126.
[39] E. Baciocchi, T. Del Giacco, F. Elisei, M.F. Gerini, M. Guerra, A. Lapi, P. Liberali, Electron transfer and singlet oxygen mechanisms in the photooxygenation of dibutyl sulfide and thioanisole in MeCN sensitized by N-methylquinolinium tetrafluoborate and 9,10-dicyanoanthracene. The probable involvement of a thiadioxirane intermediate in El, J. Am. Chem. Soc. 125 (2003) 16444–16454, https://doi.org/10.1021/ja037591o.
[40] A.D. McNaught, A. Wilkinson, IUPAC compendium of chemical terminology, Stern–Volmer Kinetic Relationships, Blackwell Scientific Publications, Oxford, 1997, https://doi.org/10.1351/goldbook.S06004 1997.
[41] D. Rehm, A. Weller, Kinetics of fluorescence quenching by electron and H-atom transfer, Isr. J. Chem. 8 (1970) 259–271, https://doi.org/10.1002/ijch.197000029.
[42] H. Yokoi, A. Hatta, K. Ishiguro, Y. Sawaki, Formation of sigma- and pi-type dimer radical cations by the photochemical one-electron oxidation of aromatic sulfides, J. Am. Chem. Soc. 120 (1998) 12728–12733, https://doi.org/10.1021/ja982595s.
[43] E. Baciocchi, T. Del Giacco, F. Elisei, M.F. Gerini, M. Guerra, A. Lapi, P. Liberali, Electron transfer and singlet oxygen mechanisms in the photooxygenation of dibutyl sulfide and thioanisole in MeCN sensitized by N -methylquinolinium tetrafluoborate and 9,10-dicyanoanthracene. The probable involvement of a thiadioxirane intermediate in electron transfer photooxygenations, J. Am. Chem. Soc. 125 (2003) 16444–16454, https://doi.org/10.1021/ja037591o.
[44] S.M. Bonesi, I. Manet, M. Freccero, M. Fagnoni, A. Albini, Photosensitized oxidation of sulfides: discriminating between the singlet-oxygen mechanism and electron transfer involving superoxide anion or molecular oxygen, Chem. - A Eur. J. 12 (2006) 4844–4857, https://doi.org/10.1002/chem.200501144.